Structural Engineering and Mechanics, *Vol. 70, No. 6 (2019) 711-722*
DOI: https://doi.org/10.12989/sem.2019.70.6.711

Buckling analysis of arbitrary point-supported plates using new hp-cloud shape functions

Sajad Jamshidi[1] and N. Fallah*[2]

[1]Department of Civil Engineering, University of Guilan, Rasht, Iran
[2] Faculty of Civil Engineering, Babol Noshirvani University of Technology, Babol, Iran

(Received January 15, 2019, Revised March 13, 2019, Accepted March 17, 2019)

Abstract. Considering stress singularities at point support locations, buckling solutions for plates with arbitrary number of point supports are hard to obtain. Thus, new Hp-Cloud shape functions with Kronecker delta property (HPCK) were developed in the present paper to examine elastic buckling of point-supported thin plates in various shapes. Having the Kronecker delta property, this specific Hp-Cloud shape functions were constructed through selecting particular quantities for influence radii of nodal points as well as proposing appropriate enrichment functions. Since the given quantities for influence radii of nodal points could bring about poor quality of interpolation for plates with sharp corners, the radii were increased and the method of Lagrange multiplier was used for the purpose of applying boundary conditions. To demonstrate the capability of the new Hp-Cloud shape functions in the domain of analyzing plates in different geometry shapes, various test cases were correspondingly investigated and the obtained findings were compared with those available in the related literature. Such results concerning these new Hp-Cloud shape functions revealed a significant consistency with those reported by other researchers.

Keywords: elastic buckling; point-supported plates; hp-cloud shape functions; Kronecker Delta property; arbitrary shape

1. Introduction

Flat plates located on columns in bearing systems as well as common connections of plates with screws, bolts, and rivets are known as practical examples of plates containing point supports. Furthermore; since welded plates provide a large amount of local stiffness at welding points, spot-welded plates have been modeled in some studies as point-supported ones (Bapat and Venkatramani 2010, Tripathy and Suryanarayan 2008). Due to the concentrated shear force and moment at the location of point supports, satisfaction of equilibrium conditions at such locations are not assumed straightforward. The application of analytical methods and the use of impulse and flexibility functions for buckling solutions targeting point-supported plates are also limited to solution of problems having simple geometry and boundary conditions Nowacki (1953).

Following the development of powerful computers, numerical methods have further advanced for solving complex problems in the last decades (Dastjerdi 2016, Chen *et al.* 2016). In this respect, (Tan *et al.* 1983) carried out an extensive study on buckling of various shapes of clamped and simply supported triangular plates under in-plane unilateral and bilateral pressure and shear loads using finite element method with six-node triangular quadratic polynomial elements Irons (1969). Moreover, (Venugopal *et al.* 1989) made used of a high-precision triangular element for stability analysis of rectangular plates with four corner-point supports. Within the finite element method, significant time and precision could be spent for creating and choosing an appropriate mesh on the problem domain. It is noted that mesh generation refers to a process for discretizing a problem geometry using a proper element. Therefore, elements overlapping each other and those not covering any region of the problem domain are not allowed during mesh generation process. Alongside mesh generation, it is even necessary to know how the elements are connected to each other in order to form up a system of equations in the finite element method Liu and Gu (2005). Furthermore, the cost of mesh generation can be higher for plates with complicated geometry shapes especially for three-dimensional domains. For the aforementioned reasons, mesh-free methods have been developed in the last two decades (Tsiatas and Yiotis 2013, Zhang and *et al.* 2014, Naghsh *et al.* 2018, Do and Lee 2018). According to these methods, there is no need to predefine a mesh on the problem domain in order to extract a system of equations. The problem domain is also discretized to a set of points in most of the meshless methods in order to model the volume and the boundary of a problem in a way that there is no requirement to define the element type and also get involved in the challenge of element connections compared with the finite element methods. In this regard, Wang and Liew (1994) further solved elastic buckling of triangular plates with arbitrary boundary conditions and intermediate line support under uniform in-plane pressure via complete polynomial shape functions and the Ritz method. As well, (Saadatpour *et al.* 1998) employed the Lagrangian shape functions and the mesh-free Galerkin method (Belytschko

*Corresponding author, Professor
E-mail: fallah@nit.ac.ir

ISSN: 1225-4568 (Print), 1598-6217 (Online)

et al. 1994) for buckling analysis of general quadrilateral-shaped elastic plates with internal line supports. Lei and Zhang (2018) used the meshless Kp-Ritz method to obtain the buckling solution of cracked hybrid laminated plates. Besides, Krysl and Belytschko (1995) analyzed thin plates using the mesh-free Galerkin method in which the moving least squares method was utilized for constructing approximate functions while the method of Lagrange multiplier was employed to meet boundary conditions Lancaster and Salkauskas (1981). (Topal *et al.* 2018) proposed the Rayleigh-Ritz method with novel plate buckled shape function for obtaining the shear buckling load of laminated plates resting on Pasternak foundation. (Garcia *et al*. 2000) also conducted a study on the Mindlin thick plate through the Hp-Cloud approximation method to prevent shear locking phenomenon Duarte and Oden (1995). The Hp-Cloud shape functions were similarly developed by (Jamshidi *et al.* 2015) for calculating neutral frequencies of arbitrary shape point-supported plates. Furthermore, (Li *et al*. 2016) introduced a new analytical method i.e. simplistic superposition method for the free vibration of rectangular thin plates resting on multiple-point supports.

Buckling as a major cause of failure in the structures is always a matter of interest for researchers. Kadari used a new hyperbolic plate theory for buckling analysis of embedded orthotropic nanoplates (Kadari *et al*. 2018). Many studies have also been done for buckling solution of functionally graded plates by developing the shear deformation theory (Meziane *et al*. 2014, Abdelaziz *et al*. 2017) and the refined plate theory (Bellifa *et al*. 2017, Bourada *et al*. 2018). Thermal buckling as another concern was investigated in cross-ply laminated and functionally graded sandwich plates with simplified higher-order shear deformation plate theory (HSDT) (Menasria *et al*. 2017, Chikh *et al*. 2017).

It should be noted that the Hp-Cloud method has been recently considered as an appropriate mesh-free one owing to some properties such as: 1) increasing continuity of approximation via proper weighting and enrichment functions; 2) improving accuracy and quality of approximation through changing influence domain of nodal points (h-refinement) and enrichment functions (p-refinement); as well as 3) having compact support property producing narrow-band matrix type of coefficient matrix.

As a whole, new Hp-Cloud shape functions with Kronecker delta property (HPCK) were used in the present paper to solve the elastic buckling of point-supported thin plates. It should be further noted that the HPCK shape functions were constructed by considering the special conditions for influence radii and selected enrichment functions of nodal points, as discussed in Section 2. Employing HPCK shape functions, it is easy to satisfy boundary conditions compared with other meshless shape functions deprived of Kronecker delta property. HPCK shape functions give smoother results for calculated stresses in comparison with other meshless shape functions. HPCK shape functions also need less computational effort for achieving the appropriate accuracy because of using less nodal points, integrating on the smaller domain (subscription surface of clouds) and producing the narrow band stiffness matrix. Based on observed HPCK shape functions capabilities, it can be utilized with higher order plate theories for buckling investigation of plates with other type of materials like orthotropic and FGM in future works.

This paper was outlined as follows. The construction procedure of new HPCK shape function was mentioned in Section 2. The governing equations of thin plate buckling analysis and eigenvalue form of the achieved set of equations obtained from the Ritz method were then discussed in Section 3. In section 4, different types of test cases were solved to demonstrate the capability of the new HPCK shape functions. Moreover; point supports were distributed on the edges of plates with various shapes for the modeling of clamped and simply boundary conditions wherein buckling coefficients were obtained with good accuracy for validation purposes. The buckling modes were also plotted to visualize the given results. In addition, interactions of in-plane forces were examined on various shapes of quadrilateral corner-supported plates.

2. A new HPCK shape function

The HPCK shape functions introduced by (Jamshidi *et al.* 2015) were developed in this paper using different samples and shapes of influence domain and enrichment functions. In the present paper, appropriate exponential and polynomial functions were also proposed as enrichment ones. Rectangular influence domain with variable influence radii were further used to achieve the Kronecker delta property along with more accurate and faster numerical integration, which led to a robust and stable solution procedure. The corresponding issues about the introduced shape functions were expressed as follows.

It is required to distribute a set of nodal points $\mathbf{Q}_n$ on the plate surface Ω for constructing the Hp-Cloud shape functions, such that Duarte and Oden (1995):

$$\mathbf{Q}_n = \{\mathbf{x}_1, \mathbf{x}_2, \ldots, \mathbf{x}_n\} \; ; \; \mathbf{x}_\alpha \in \Omega \tag{1}$$

Where $\mathbf{x}_\alpha$ is the coordinates of the nodal points on the problem domain. A rectangular influence area ω_α is also defined for each nodal point via the influence radii in x direction $h_{\alpha x}$ and y direction $h_{\alpha y}$. This rectangular domain ω_α is called cloud of the node $\mathbf{x}_\alpha$ and the assembly of clouds of all nodal points must cover the entire problem domain. Considering $(\underline{x,y})$ is the coordinate of the arbitrary point; then, ω_α is defined as:

$$\omega_\alpha = \{y \in \Omega : |x_\alpha - x| < h_{\alpha x} \, , |y_\alpha - y| < h_{\alpha y}\} \tag{2}$$

$$\Omega \subset \bigcup_{\alpha=1}^{n} \omega_\alpha \tag{3}$$

Likewise, the Hp-Cloud approximated function can be written as follows:

$$w^{\mathrm{hp}}(\mathbf{x}) = \sum_{\alpha=1}^{n} \sum_{i=1}^{m_\alpha} w_{\alpha i} (\psi_\alpha(\mathbf{x}) L_{\alpha i}(\mathbf{x})) \tag{4}$$

Wherein n is the number of nodal points, $w_{\alpha i}$ stands for the unknown coefficient, $\psi_\alpha(\mathbf{x})$ shows the partition of unity function, $L_{\alpha i}(\mathbf{x})$ is the enrichment function (Yosida 1978, Melenk and Babuska 1996), and m_α refers to the number of monomials in the enrichment function of point $\mathbf{x}_\alpha$. As a whole, the following conditions must be met by the selected partition of unity functions:

$$\begin{aligned}&\psi_\alpha(\mathbf{x}) \in C_0^s(\omega_\alpha); \quad s \geq 0; \quad 1 \leq \alpha \leq n\\ &\sum_{\alpha=1}^{n} \psi_\alpha(\mathbf{x}) = 1 \; ; \quad \forall\, \mathbf{x} \in \Omega\end{aligned} \tag{5}$$

In the present paper, the Shepard function accommodating the conditions expressed in Eq. (5) was used as the partition of unity part of approximated function for nodal points Shepard (1968). Choosing the Shepard function, less computational effort was required to make compared with other ones like the moving least squares method. The Shepard function is stated by Eq. (6):

$$\psi_\alpha(\mathbf{x}) = \frac{W_\alpha(\mathbf{x})}{\sum_\beta W_\beta(\mathbf{x})} \tag{6}$$

In which β denotes the clouds that include point $\mathbf{x}$ and $W_\alpha(\mathbf{x})$ is the weight function of nodal point $\mathbf{x}_\alpha$. This weight function defined for all nodal points on the plate must also fulfill the relations in Eq. (7):

$$\begin{aligned}&W_\alpha(\mathbf{y}) \geq 0 \quad \forall\, \mathbf{y} \in \Omega\\ &W_\alpha(\mathbf{y}) := W_\alpha(\|\mathbf{x}_\alpha - \mathbf{y}\|)\end{aligned} \tag{7}$$

In which $W_\alpha(\mathbf{y})$ is the distance function giving a positive quantity for points placed inside the cloud ω_α and is also equal to zero for the points located out of the cloud ω_α. Based on the required continuity of the thin plate buckling problem which is C^1 continuity and in order to complete smooth approximation, compact unity conditions are similarly considered for constructing the weight functions Liu and Liu (2003). The given function in (Jamshidi *et al.* 2015) was also used in this paper. Defining $R_x = |x - x_\alpha|/h_{\alpha x}$ and $R_y = |y - y_\alpha|/h_{\alpha y}$, the weight function employed can be written as:

$$\begin{aligned}&\begin{cases} W_\alpha(R) = 1 - \frac{10}{3}R^2 + 5R^4 - \frac{8}{3}R^5 & R \leq 1\\ 0 & R > 1\end{cases}\\ &R = R_{\mathbf{x}} \times R_{\mathbf{y}}\end{aligned} \tag{8}$$

The complete polynomial and exponential functions were correspondingly used as enrichment $\mathbf{L}$ part of Hp-Cloud shape function in this paper. These types of enrichment functions could provide simplicity in computations as well as appropriate continuity.

Thus, the following two conditions must be satisfied for constructing the new HPCK shape functions: 1) influence radii of nodal points $h_{\alpha x}$, $h_{\alpha y}$ must be selected in a way that none of the other nodal points are placed in the rectangular influence domain of point $\mathbf{x}_\alpha$ as it was shown in Fig. 1; and 2) complete polynomial $\mathbf{L}_\mathrm{P}$ or exponential $\mathbf{L}_\mathrm{E}$ enrichment functions need to be used in an appropriate pattern as expressed in Eq. (9):

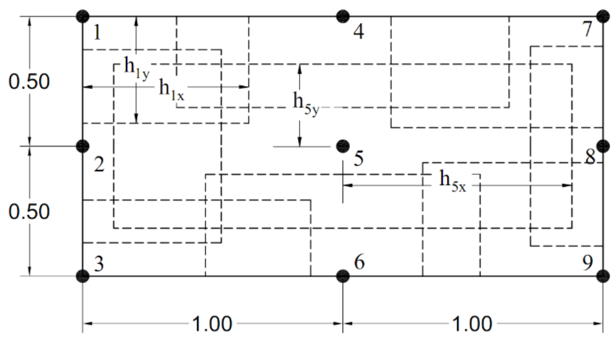

Fig. 1 Distributed nodal points and influence radii

$$\begin{aligned}&\mathbf{L}_\mathrm{P} = [1, (x - x_\alpha), (y - y), (x - x_\alpha)^2,\\ &(x - x_\alpha)(y - y_\alpha), (y - y_\alpha)^2, \ldots (y - y_\alpha)^n]\\ &\mathbf{L}_\mathrm{E} = [1, 1 - e^{(x - x_\alpha)(y - y_\alpha)}, 1 - e^{(x - x_\alpha)^2 (y - y_\alpha)2}, \ldots, 1 - e^{(x - x_\alpha)^n (y - y_\alpha)n}]\end{aligned} \tag{3}$$

Upon applying the above-mentioned two conditions, the achieved shape functions will have the Kronecker delta property. So, it is not required to use the method of Lagrange multiplier to satisfy the Dirichlet boundary conditions.

To visualize the discussed issues about constructing the HPCK shape functions, a rectangular domain shown in Fig. 1 was also considered. As an appropriate choice, the influence radii of all the nodal points illustrated in Fig. 1 can be selected as $h_{\alpha x} = 1$, $h_{\alpha y} = 0.5$ to meet the first condition of constructing the HPCK shape functions. The complete polynomial of order two with proposed pattern in Eq. (9) was also used in this example as enrichment function for all nodal points. After applying these assumptions, the Hp-Cloud approximation quantity $w(\mathbf{x})$ in arbitrary point $\mathbf{x} = \mathbf{x}_3$ is expressed by:

$$w(\mathbf{x} = \mathbf{x}_3) = \sum_{\alpha=1}^{9} \sum_{i=1}^{6} w_{\alpha i} \left(\psi_\alpha(\mathbf{x} = \mathbf{x}_3) L_{\alpha i}(\mathbf{x} = \mathbf{x}_3) \right) \tag{10}$$

Because of the fulfillment of the first condition in this example, point $\mathbf{x} = \mathbf{x}_3$ is just placed in the cloud of nodal point $\mathbf{x}_3$, so:

$$\begin{aligned}w(\mathbf{x} = \mathbf{x}_3) &= \sum_{i=1}^{6} w_{3i} \left(\psi_3(\mathbf{x} = \mathbf{x}_3) L_{3i}(\mathbf{x} = \mathbf{x}_3) \right)\\ &= \sum_{i=1}^{6} w_{3i} \left(\frac{\psi_3(\mathbf{x} = \mathbf{x}_3)}{\sum_\beta W_\beta(\mathbf{x} = \mathbf{x}_3)} L_{3i}(\mathbf{x} = \mathbf{x}_3) \right)\end{aligned} \tag{11}$$

Arbitrary nodal point weight function value $W_\beta(\mathbf{x})$,(β =1 to 10) in $\mathbf{x} = \mathbf{x}_3$ is similarly calculated by Eq. (12):

$$\begin{cases} W_\beta(\mathbf{x} = \mathbf{x}_3) = 0 & \beta \neq 3\\ W_\beta(\mathbf{x} = \mathbf{x}_3) = 1 & \beta = 3\end{cases} \tag{12}$$

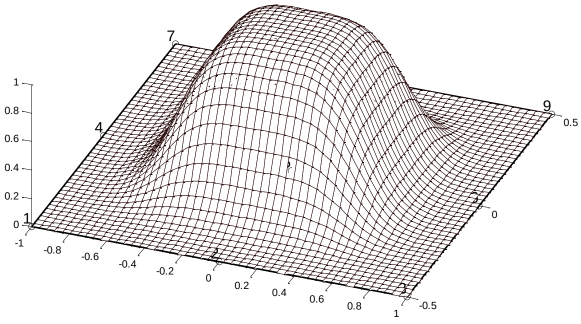

Fig. 2 Changes of $\phi_{51} = \psi_5 L_{51}$ in the example domain

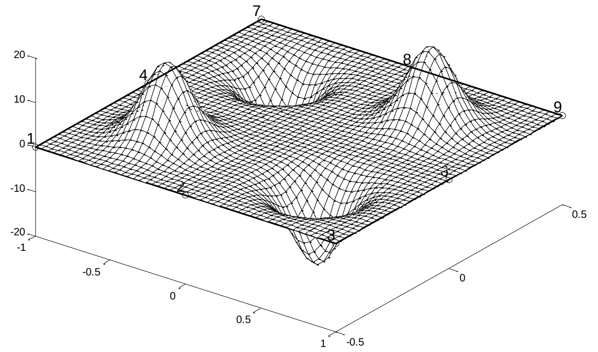

Fig. 3 Changes of $\frac{\partial^2 \phi_{51}}{\partial x \partial y} = \frac{\partial^2 (\psi_5 L_{51})}{\partial x \partial y}$ in the example domain

According to Eq. (12), the partition of unity in $\mathbf{x} = \mathbf{x}_3$ is obtained as $\psi_3(\mathbf{x}=\mathbf{x}_3)=1$. Moreover, the enrichment function part in $\mathbf{x} = \mathbf{x}_3$ is $L_3(\mathbf{x}=\mathbf{x}_3) = [1,0,0,0,0,0]$. Finally, the following changes can be observed from Eq. (13) for $w(\mathbf{x}=\mathbf{x}_3)$:

$$w(\mathbf{x} = \mathbf{x}_3) = w_{31} \tag{13}$$

It was demonstrated that $w(\mathbf{x}=\mathbf{x}_\gamma)= w_{\gamma 1}, (\gamma = 1,2,\dots,9)$ for all nodal points of the given example. Accordingly, it is clear that the achieved shape functions are endowed with Kronecker delta property. In order to visualize the results, the shape functions of some nodal points of this example and its derivatives were presented in Figs. 2-5.

In this paper, the proposed HPCK shape functions were utilized to solve the buckling of various shapes of point-supported plates. The obtained results, presented in Section 4, also demonstrated proper precision and fast convergence of the given method involving the proposed shape functions.

3. Buckling analysis

The linear strains of a plate can be determined using classical thin plate theory. Employing the obtained stress and strain relations of elastic materials in energy equation, the strain energy can be expressed as follows:

$$\mathrm{U} = \frac{D}{2}\int_{\mathrm{A}} \left(\left(\frac{\partial^2 w}{\partial x^2} + \frac{\partial^2 w}{\partial y^2} \right)^2 - 2(1-\nu)\left(\frac{\partial^2 w}{\partial x^2}\frac{\partial^2 w}{\partial y^2} - \left(\frac{\partial^2 w}{\partial x \partial y} \right)^2 \right) \right) dA \tag{14}$$

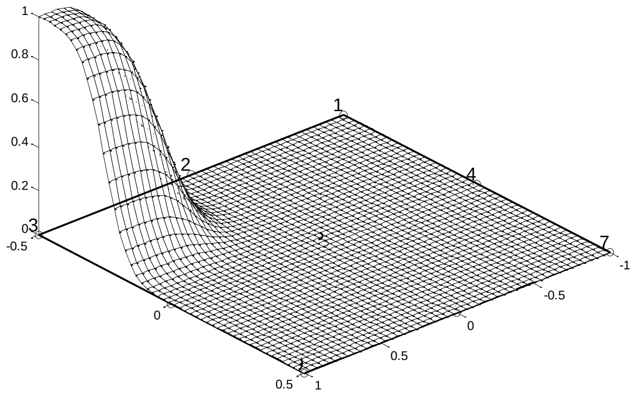

Fig. 4 Changes of $\phi_{31} = \psi_3 L_{31}$ in the example domain

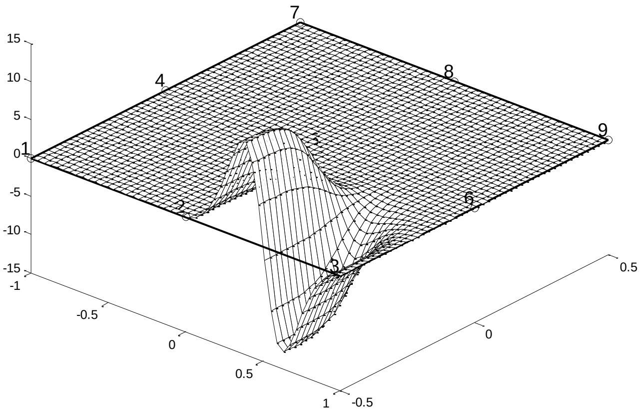

Fig. 5 Changes of $\frac{\partial^2 \phi_{31}}{\partial x \partial x} = \frac{\partial^2 (\psi_3 L_{31})}{\partial x \partial x}$ in the example domain

In which $\boldsymbol{\nu}$ is the Poisson's ratio and D shows the flexural rigidity Szilard (2004). Determining the non-linear strain of applied in-plane loads shown in Fig. 6, the potential of corresponding external forces can be stated as:

$$\begin{aligned} \mathrm{V} &= -\frac{1}{2}\int_A \left[N_x \left(\frac{\partial w}{\partial x} \right)^2 + N_y \left(\frac{\partial w}{\partial y} \right)^2 + 2N_{xy}\left(\frac{\partial w}{\partial x} \right)\left(\frac{\partial w}{\partial y} \right) + N_0 \left(\frac{y}{\mathrm{b}} \right)\left(\frac{\partial w}{\partial x} \right)^2 \right] \mathrm{d}A \\ &= -\frac{\lambda}{2}\int_A \left[\overline{N}_x \left(\frac{\partial w}{\partial x} \right)^2 + \overline{N}_y \left(\frac{\partial w}{\partial y} \right)^2 + 2\overline{N}_{xy}\left(\frac{\partial w}{\partial x} \right)\left(\frac{\partial w}{\partial y} \right) + \overline{N}_0 \left(\frac{y}{\mathrm{b}} \right)\left(\frac{\partial w}{\partial x} \right)^2 \right] \mathrm{d}A \end{aligned} \tag{15}$$

Wherein λ stands for buckling coefficient. If the point supports are not placed on the nodal points, then the method of Lagrange multipliers is used to satisfy the zero deflection conditions in the place of corresponding point supports as follows:

$$\Pi_{\mathrm{a}} = \Pi + \sum_r \Gamma_r w\big|_{x=x_r, y=y_r} = \mathrm{U} + \mathrm{V} + \sum_r \Gamma_r w\big|_{x=x_r, y=y_r} \tag{16}$$

In which $\prod$ is the total energy, $\prod_{\mathrm{a}}$ refers to the augmented energy functional, (x_r, y_r) indicates the location of the point supports, and Γ_r shows the Lagrange multipliers. Assuming that the plate has only s continuous simply supported boundary conditions and t continuous clamped ones, the augmented energy functional $\prod_{\mathrm{a}}$ can be rewritten as:

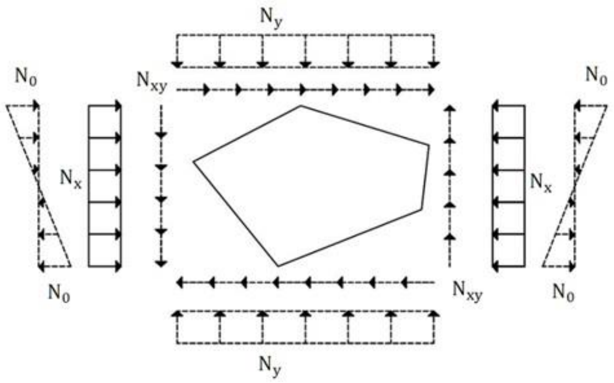

Fig. 6 A Plate with arbitrary shape under in-plane loads

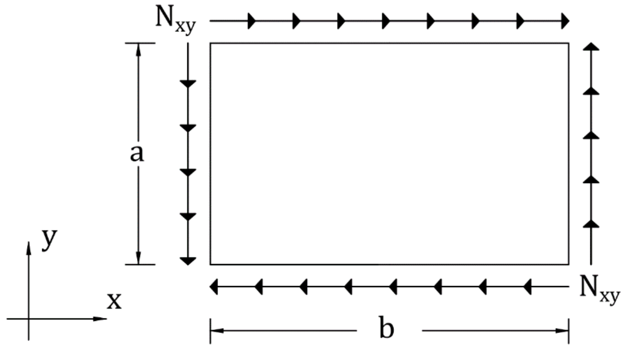

Fig. 7 Rectangular plate under pure shear force

$$\Pi_a = \Pi + \frac{1}{2}\left(\sum_s \Gamma_s \int_{\Lambda_s} w^2 \mathrm{d}\Lambda + \sum_t \Gamma_t \int_{\Lambda_t} \left(\frac{\partial w}{\partial n_t}\right)^2 \mathrm{d}\Lambda\right) \quad (17)$$

Where Γ_s and Γ_t are the Lagrange multipliers, Λ_s is the s^{th} simple boundary, Λ_t shows the t^{th} clamped boundary, and n_t refers to the normal boundary Λ_s. In order to attain the neutral equilibrium and stationary state, the Ritz method was applied to Eq. (16) as follows:

$$\delta\Pi_a = 0 \rightarrow \frac{\partial \Pi_a}{\partial w_{\alpha i}} = 0, \frac{\partial \Pi_a}{\partial \Gamma_r} = 0 \quad (18)$$

Eq. (18) was then transformed to the following eigenvalue problem:

$$\left(\begin{bmatrix} \mathbf{K} & \mathbf{P} \\ \mathbf{P}^{\mathrm{T}} & \mathbf{0} \end{bmatrix} - \lambda \begin{bmatrix} \mathbf{K_G} & 0 \\ 0 & \mathbf{0} \end{bmatrix}\right)\begin{Bmatrix} \overline{\mathbf{w}} \\ \mathbf{\Gamma} \end{Bmatrix} = \begin{Bmatrix} \mathbf{0} \\ \mathbf{0} \end{Bmatrix} \quad (19)$$

In which $\mathbf{K}$ and $\mathbf{K}_{\mathrm{G}}$ are respectively the elastic and the geometric stiffness matrices, $\overline{w}$ shows the unknown coefficient vector and $\mathbf{\Gamma}$ stands for the Lagrange multipliers vector. The components of the $\mathbf{K}$, $\mathbf{K}_{\mathrm{G}}$ and P matrices can be also expressed as:

$$\begin{aligned}
\mathrm{K}_{m\times(\alpha-1)+i,m\times(\beta-1)+j} = D\int_{\omega_\alpha \cap \omega_\beta} &\left(\frac{\partial^2(\psi_\alpha L_{\alpha i})}{\partial x^2}\left(\frac{\partial^2(\psi_\beta L_{\beta j})}{\partial x^2} + \nu\frac{\partial^2(\psi_\beta L_{\beta j})}{\partial y^2}\right)\right. \\
&+ \frac{\partial^2(\psi_\alpha L_{\alpha i})}{\partial y^2}\left(\frac{\partial^2(\psi_\beta L_{\beta j})}{\partial y^2} + \nu\frac{\partial^2(\psi_\beta L_{\beta j})}{\partial x^2}\right) \\
&\left. + 2(1-\nu)\frac{\partial^2(\psi_\alpha L_{\alpha i})}{\partial x\partial y}\frac{\partial^2(\psi_\beta L_{\beta j})}{\partial x\partial y}\right)dA \\
\mathrm{K}_{\mathrm{G}_{m\times(\alpha-1)+i,m\times(\beta-1)+j}} = -\lambda\int_{\omega_\alpha \cap \omega_\beta} &\left(\left(\overline{N}_x + \overline{N}_0\frac{y}{\mathrm{b}}\right)\frac{\partial(\psi_\alpha L_{\alpha i})}{\partial x}\frac{\partial(\psi_\beta L_{\beta j})}{\partial x}\right. \\
&+ \overline{N}_y\frac{\partial(\psi_\alpha L_{\alpha i})}{\partial y}\frac{\partial(\psi_\beta L_{\beta j})}{\partial y} + \overline{N}_{xy}\frac{\partial(\psi_\alpha L_{\alpha i})}{\partial x}\frac{\partial(\psi_\beta L_{\beta j})}{\partial y} \\
&\left. + \overline{N}_{xy}\frac{\partial(\psi_\beta L_{\beta j})}{\partial x}\frac{\partial(\psi_\alpha L_{\alpha i})}{\partial y}\right)dA \\
\mathrm{P}_{m\times(\alpha-1)+i,r} = (\psi_\alpha L_{\alpha i})&\big|_{x=x_r,y=y_r}
\end{aligned} \quad (20)$$

It should be noted that the smallest positive value of eigenvalues of Eq. (19) is called the buckling load. The results are also presented in a dimensionless format such that:

$$k_{a1} = \frac{N_x b^2}{\pi^2 D}, \; k_{a2} = \frac{N b^2}{\pi^2 D}, \; k_s = \frac{N_{xy} b^2}{\pi^2 D}, \; k_b = \frac{N_0 b^2}{\pi^2 D} \quad (21)$$

Wherein k_{a1}, k_{a2}, k_s and k_b are respectively the buckling coefficients corresponding to the uniaxial pressure, biaxial pressure ($N_x = N_y = N$), as well as shear and bending load cases; D shows the flexural rigidity of plate, and b refers to the plate length parameter.

Integration domain in the Hp-Cloud method as displayed in Eq. (20) is the subscription surface of two corresponding clouds. These integration domains are rectangular except in cases in which subscription surfaces intersect the boundaries. The cell structure method (Suwranu and Bathe 2000, Bathe and Suwranu 2001, Suwranu and Bathe 2001) and refined cell structure method (Jamshidi *et al.* 2015) were also used in this paper as a numerical integration method for calculating the mentioned integrations.

4. Numerical results

In order to show the efficiency and the accuracy of the shape functions, proposed in the present paper, various examples including different geometry shapes were presented in the following section. These specific configurations of point supports were selected just for comparison and verification purposes with those existing in reliable literature. The proposed method could be used for arbitrary distribution of point supports.

4.1 Rectangular plate

4.1.1 Rectangular plates with simply support under shear loading

Elastic buckling of rectangular plates with simply support under shear loading shown in Fig. 7 was examined in terms of different aspect ratios. So, the HPCK shape functions were constructed by distributing n_x and n_y points along the length and the width of the plate. The shear buckling coefficient (k_s) defined by Eq. (21) were also obtained and compared with those reported by (Saadatpour *et al.* 1998) and Allen and Bulson (1980) in Table 1, and

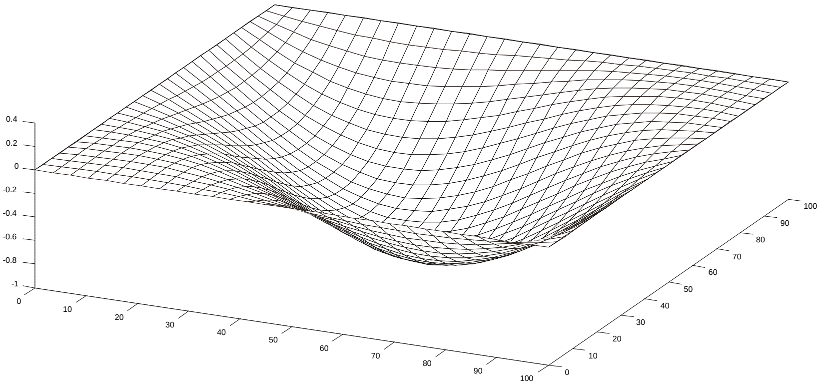

Fig. 8 Buckling mode shape of simply supported rectangular plate under pure shear

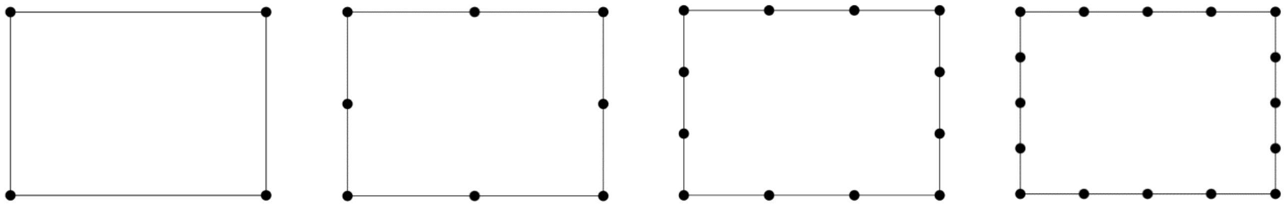

(a) (b) (c) (d)

Fig. 9 Periodic distributing of one-row point supports along edges of rectangular plate

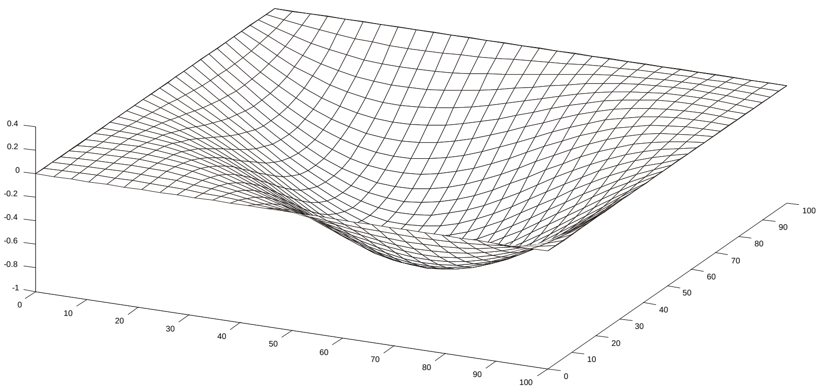

Fig. 10 Uniaxial pressure buckling mode shape of square plate by point supports displayed in Fig. 9(d)

Table 1 Shear buckling coefficients k_s of simply supported rectangular plates

a/b	1	1.2	1.4	1.5	1.6	1.8	2
$n_y \times n_x$	10×10	10×12	10×14	10×15	10×16	10×18	10×20
Allen and Bulson (1980)	9.34	8.00	7.30	7.11	6.91	6.80	6.6
(Saadatpour *et al.* 1998)	9.32	8.04	7.29	7.08	6.92	6.70	6.57
Present Study	9.3204	8.0257	7.2941	7.0811	6.9231	6.7028	6.5716

consequently a good agreement was observed. Moreover, the shear buckling mode shape of the square plate was presented in Fig. 8.

4.1.2 Rectangular plates supported by point supports

Elastic buckling of rectangular plates with aspect ratios of a/b = 1,1.5 and 2 and point support arrangement shown in Fig. 9 were investigated in the present section. The calculated buckling coefficients introduced in Eq. (21) were then presented in Table 2. As it was observed, the buckling coefficients given in Table 2 were in good agreement with the results from the related literature. According to Table 2, the values of k_{a1} for square plate (a/b =1) got close to the corresponding value for a square plate with simply supports (k_{a1} =4) through increasing the point supports Szilard (2004). The value of k_{a1} for square plate with point support configuration shown in Fig. 9 was obtained as 3.9562 and its relevant buckling mode shape was presented in Fig. 10.

Table 2 Buckling coefficients of rectangular plates with point supports shown in Fig. 9

	$\gamma = \frac{a}{b}$	k_{a1} Present study	k_{a1} Hedayati (2007)	k_{a2} Present study	k_{a2} Hedayati (2007)	k_s Present study	k_s Hedayati (2007)	k_b Present study	k_b Hedayati (2007)
	1.0	0.9219	0.9217a	0.7391	0.7390[a]	1.3480	-	2.5072	-
Fig. 9(a)	1.5	0.4099	-	0.3921	-	0.9525	-	1.5300	-
	2.0	0.2304	-	0.2258	-	0.7677	-	1.1095	-
	1.0	3.4600	3.52	1.9713	-	4.0065	4	6.9100	6.91
Fig. 9(b)	1.5	1.7062	-	1.4210	-	2.5403	-	3.7749	-
	2.0	0.9509	0.95	0.9292	-	1.8543	1.87	2.5572	2.55
	1.0	3.8759	3.95	1.9949	-	6.9619	7.01	13.4861	13.48
Fig. 9(c)	1.5	3.5884	-	1.4398	-	4.7879	-	6.9942	-
	2.0	2.1710	2.17	1.2464	-	3.0963	3.16	4.5309	4.53
	1.0	3.9562	3.99	1.9989	-	8.2814	8.51	22.1000	22.14
Fig. 9(d)	1.5	4.1100	-	1.4429	-	6.0091	-	11.1786	-
	2.0	3.5324	3.75	1.2489	-	4.6726	5.08	7.0396	7.04

[a]Reported in (Venugopal *et al.* 1989)

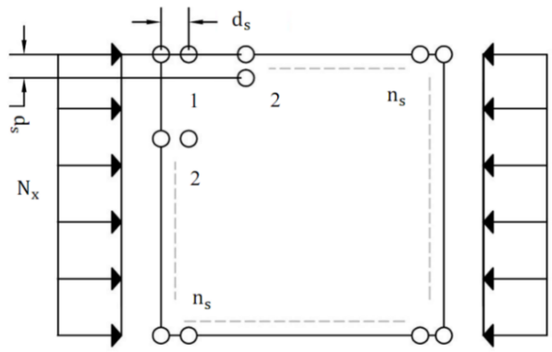

Fig. 11 Square plate with distributing two-row point supports on its edges under uniaxial pressure buckling load

Table 3 Uniaxial pressure buckling coefficients of square plate presented in Fig. 11

n_s	5	5	5	4	4
d_s	$a/15$	$a/18$	$a/20$	$a/15$	$a/12.5$
k_{a1}	11.1086	10.6256	10.3557	9.5949	10.11
k_{a1}^c	10.08	10.08	10.08	10.08	10.08

Theoretically, it would be possible to model fully clamped or simply supported plates by choosing a proper point support arrangement. The values of k_{a1} for square plate and point support configuration shown in Fig. 11 are expressed in Table 3. In order to model the clamped boundary condition using the proper distribution of point supports, the achieved buckling coefficients k_{a1} for the plate are compared with $k_{a1}^c = 10.08$ that is the corresponding buckling coefficient for a fully clamped square plate Allen and Bulson (1980). It is obvious from the presented results in Table 3 that the distribution of four pairs of point supports along the edges of the plate with distance of $a/12.5$ from each other can be considered as the proper equivalent point support configuration of the clamped boundary condition. The corresponding buckling mode shape was illustrated in Fig. 12.

Table 4 Buckling coefficients k_c of rhombic plate illustrated in Fig. 13

n_s	α 30°	36°	45°	60°
5	3.7059	4.8738	7.5723	17.9447
6	3.7151	4.8814	7.6273	18.6352
7	3.7203	4.8854	7.6615	18.9813
8	3.7210	4.8855	7.6642	19.1477

4.2 Rhombic plate

The HPCK shape function is used to calculate the critical buckling load of rhombic plate via distributed point supports presented in Fig. 13. The buckling coefficients k_c given in Eq. (22) were calculated and the results were reported in Table 4.

$$k_c = \frac{N_y (2a\sin\alpha)^2}{\pi^2 D} \tag{22}$$

The small increase in the buckling load coefficient when the point support numbers are greater than $n_s = 7$ indicates that the plate boundary condition approaches the corresponding fully simply supported boundary condition as point supports along the edges of rhombic plate are added.

4.3 Skew plate

The buckling of skew plate under uniaxial pressure and distributed point supports shown in Fig. 14 was examined in the present section. The plate buckling coefficients were also obtained according to Eq. (23) and the results were presented in Table 5.

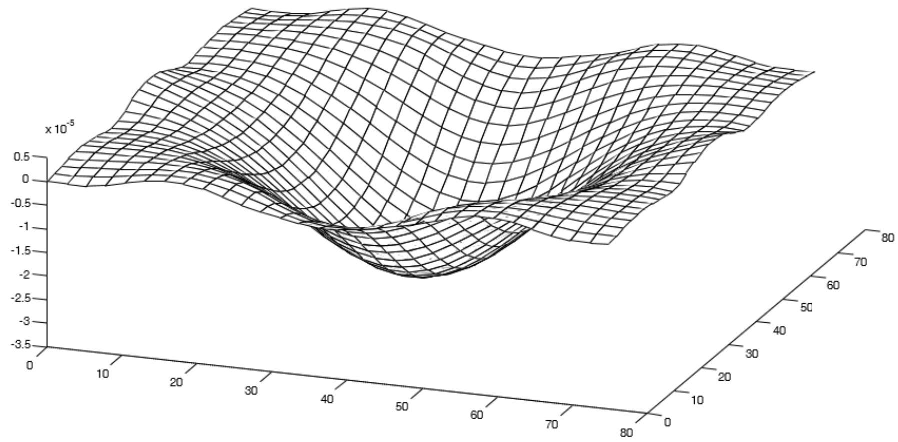

Fig. 12 Uniaxial pressure buckling mode shape of square plate shown in Fig. 11 with $n_s = 4$, $d_s = a/12.5$

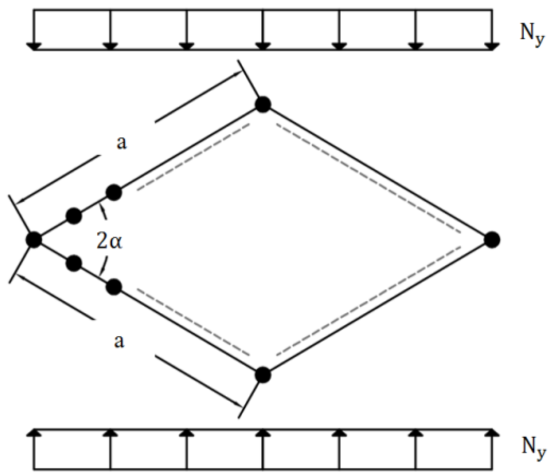

Fig. 13 Rhombic plate with periodic distribution of point supports along its edges under in-plane uniaxial pressure load N_y

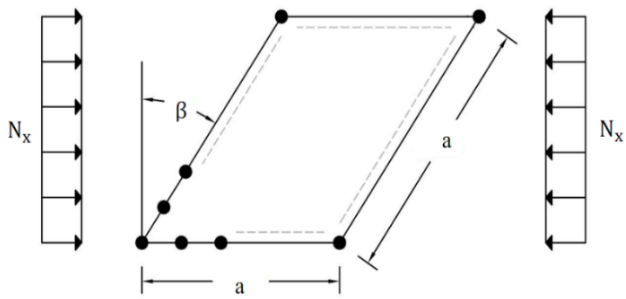

Fig. 14 A skew plate with periodic distribution of point supports along its edges under in-plane uniaxial pressure load assigned by N_x

The results presented in Table 5 suggested that the magnitudes of buckling coefficient approached the buckling coefficient of fully simply supported skew plate through increasing the point supports along the edges of the skew plate (Saadatpour *et al.* 1998).

$$k_c = \frac{N_x a^2}{\pi^2 D}(\cos\beta)^4 \tag{23}$$

Table 5 Buckling coefficients k_c of skew plate shown in Fig. 14

n_s	β				
	0°	15°	20°	30°	45°
5	3.9562	3.7381	3.5693	3.0997	2.1085
6	3.9840	3.7991	3.6462	3.1815	2.227
7	3.9903	3.8085	3.6600	3.2344	2.2799
Saadatpour *et al.* (1998)	4	3.834	-	3.301	2.439

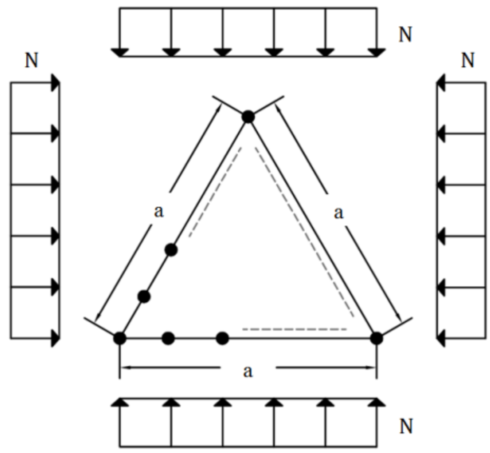

Fig. 15 An equilateral triangular plate with n_s point supports along its edges under biaxial pressure

4.4 Triangular plate

Triangular plates have wide applications in industry, so that the HPCK shape functions are used to calculate the buckling load of various shapes of triangular plates in which the point supports along the plate edges are distributed.

4.4.1 Equilateral triangular plate

The buckling load coefficient of point-supported equilateral triangular plate under biaxial pressure illustrated in Fig. 15 was calculated and presented in Table 6. The buckling load coefficient k_c is expressed by:

Table 6 Buckling load coefficients of equilateral triangular plates shown in Fig. 15

n_s	5	6
k_c	3.9470	3.9799
k_c^s Taylor (1967)	4	4

Table 7 Buckling load coefficients of right-angled isosceles triangular plates displayed in Fig. 16

n_s	5	6
K_c	4.9611	4.9850
k_c^s Wittrick (1954)	5	5

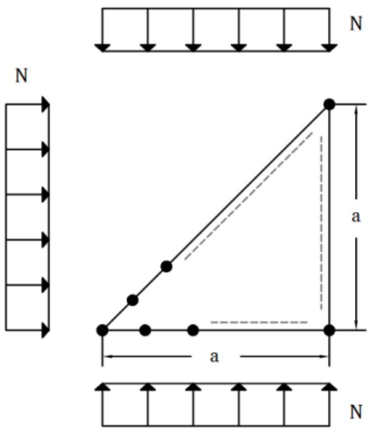

Fig. 16 Right-angled isosceles triangular plate with n_s point supports along its edges under biaxial pressure

$$k_c = \frac{3Na^2}{4\pi^2 D} \tag{24}$$

In Table 6, the obtained values of k_c were compared with those of a fully simply supported boundary condition (k_c^s = 4) Taylor (1967). According to Table 6, the buckling load coefficients of this plate with n_s = 6 point supports were reported by 99.5% of the buckling load coefficient of the corresponding fully simply supported plate.

4.4.2 Right-angled isosceles triangular plate

Exact solution of simply supported right-angled isosceles triangular plate under in-plane biaxial pressure load had been already determined by Wittrick (1954). The buckling coefficient of point-supported right-angled isosceles triangular plate presented in Fig. 16 was shown in Table 7 and compared with that in Wittrick (1954). The buckling coefficient is obtained using the following equation:

$$k_c = \frac{Na^2}{\pi^2 D} \tag{25}$$

According to Table 7, the buckling load coefficient of right-angled isosceles triangular plate with n_s = 6 was by 99.7% of the corresponding value for a fully simply supported plate ($k_c^s = 5$) Wittrick (1954).

Table 8 Buckling load coefficients of isosceles triangular plates illustrated in Fig. 17(a)

$\frac{h}{a}$	n_s 5	6	(k) Irons (1969)
1	14.648	14.8419	14.926
1.25	11.9645	12.1717	-
1.5	10.3794	10.5923	-
1.75	9.28	9.527	-
2	8.4999	8.761	8.954
2.5	7.2599	7.7272	7.976

Table 9 Buckling load coefficients of isosceles triangular plates shown in Fig. 17(b)

$\frac{h}{a}$	n_s 5	6	$\left(\frac{k}{\pi^2}\right)$ Irons (1969)
1	2.4805	2.4911	2.4998
1.25	2.9391	2.9598	2.9674
1.5	3.4387	3.4671	3.4825
1.75	3.9858	4.021	4.04
2	4.5806	4.6184	4.6426
2.5	5.8971	5.9383	5.9698

4.4.3 Isosceles triangular plate

Elastic buckling of isosceles triangular plates under uniaxial pressure illustrated in Fig. 17(a) and biaxial pressure shown in Fig. 17(b) were studied for different values of angle α as well as numbers of point supports. In Table 8, the results of elastic buckling coefficients of isosceles triangular plates under uniaxial pressure obtained from Eq. (26) were compared with those given by the finite element method for simply supported boundary conditions Irons (1969).

$$k_c = 4\frac{Na^2}{\pi^2 D} \tag{26}$$

Furthermore, the buckling coefficients calculated by the present method with those reported for simply supported isosceles plates in Irons (1969) were compared in Table 9. The buckling coefficient is determined by:

$$k_c = \frac{Nh^2}{\pi^2 D} \tag{27}$$

Tables 8 and 9 implied that the buckling coefficients got close to the corresponding values for a fully simply supported plate as the point supports along the boundary of isosceles triangular plates were increased.

4.5 Interaction of in-plane loads for quadrilateral plates

The effect of interaction of in-plane loads on the buckling of quadrilateral plates with four corner supports was studied in the present section.

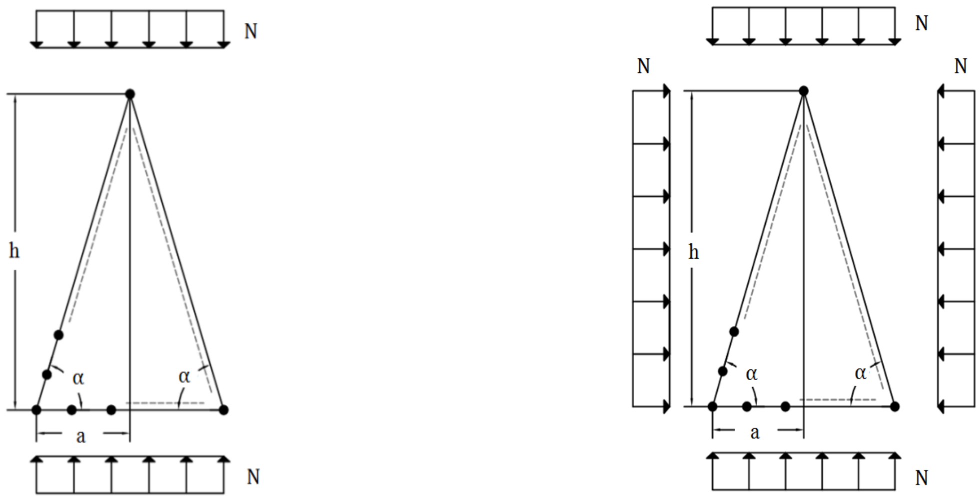

(a) (b)

Fig. 17 Isosceles triangular plate with periodic distribution of n_s point supports along its edges under a) uniaxial pressure and b) biaxial pressure

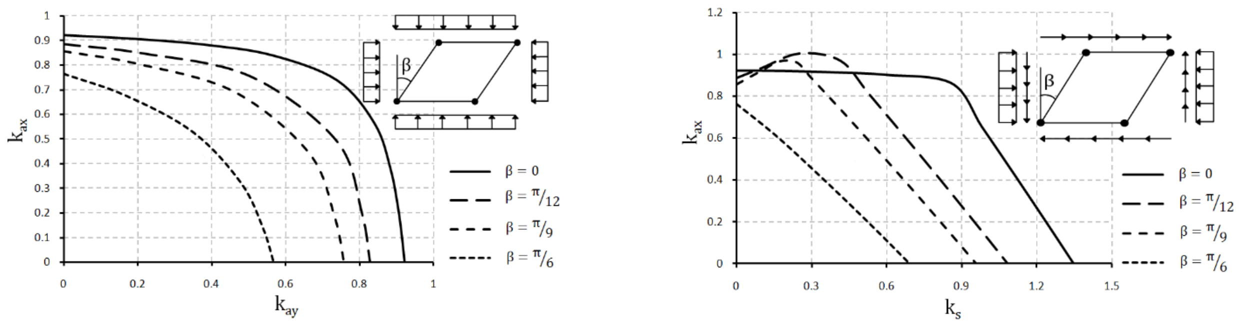

(a) (b)

Fig. 18 Interaction curves of corner-supported skew plate; a) in-plane pressure in x axis with in-plane pressure in y axis and b) in-plane pressure in x axis with in-plane shear pressure and b) biaxial pressure

4.5.1 Skew plate

The interaction curves of skew plates supported at corners with side lengths equal to α subjected to the in-plane compressive loads in both x and y directions and also in-plane compressive loads in x direction with the shear loads were obtained and presented in Figs. 18(a) and 18(b). The buckling coefficients k_{ax}, k_{ay} and k_s are calculated according to the following equations:

$$k_{ax} = \frac{N_x a^2}{\pi^2 D}(\cos\beta)^4 \ , \ k_{ay} = \frac{N_y a^2}{\pi^2 D}(\cos\beta)^4 \ , \quad k_s = \frac{N_{xy} a^2}{\pi^2 D}(\cos\beta)^4 \tag{28}$$

Fig. 18 revealed that the interaction curves of skew plates could be in different shapes for different value of β.

4.5.2 Rhombic Plate

The interaction curves of corner-supported rhombic plates with side length of α under the in-plane pressure load in x and y directions and the in-plane pressure load in x direction with the shear load were depicted in Figs. 19(a) and 19(b), respectively. The buckling coefficients are obtained from:

$$k_{ax} = \frac{N_x (2a\sin\alpha)^2}{\pi^2 D} \ , \ k_{ay} = \frac{N_y (2a\sin\alpha)^2}{\pi^2 D} \ , \quad k_s = \frac{N_{xy} (2a\sin\alpha)^2}{\pi^2 D} \tag{29}$$

Fig. 19 showed that the shape of interaction curves depended on the α similar to the skew plates.

5. Conclusions

With the aim of extracting the HPCK shape functions, the distribution of the field nodes and the selection of the proper influence radii as well as the construction of enrichment functions were discussed in the present paper. Moreover, various elastic buckling problems of point-supported plates with arbitrary shapes were investigated. It was observed that the results of the buckling coefficients approached the corresponding results of fully simply supported plates as the point supports along the boundary of plates were increased. Furthermore, a proper configuration of point supports along the boundary of square plate was investigated for the modelling of the clamped boundary condition which was consistent with the existing results in

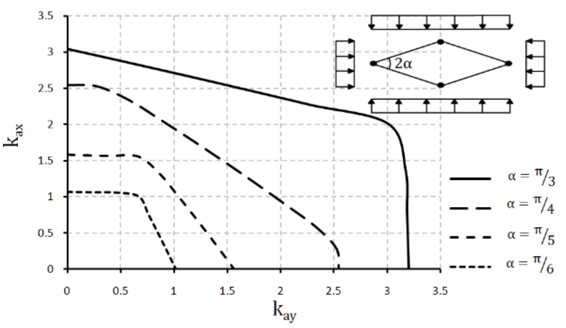

(a)

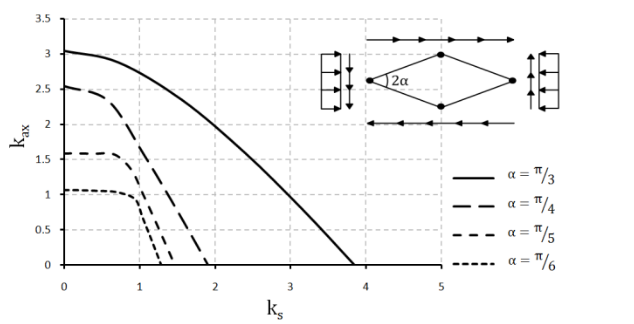

(b)

Fig. 19 Interaction curves of corner-supported rhombic plate; a) in-plane pressure in x axis with in-plane pressure in y axis and b) in-plane pressure in x axis with in-plane shear

the related literature. The findings extracted from the developed Hp-Cloud shape functions also showed a good agreement in terms of dealing with plates with point supports as important cases due to stress singularities at point support locations compared with those obtained by other researchers. In most examples provided in the present paper, the accuracy of four decimal places for calculated buckling coefficients was obtained only through 16 to 25 regularly distributed nodal points. Furthermore, the observed convergence and accuracy of the proposed HPCK shape functions confirmed it as a favorite method to examine other problems of solid mechanics.

References

Abdelaziz, H. H., Meziane, M. A. A., Bousahla, A. A., Tounsi, A., Mahmoud, S. R. and Alwabli, A. S. (2017), "An efficient hyperbolic shear deformation theory for bending, buckling and free vibration of FGM sandwich plates with various boundary conditions", *Steel Compos. Struct.*, **25**(6), 693-704. http://dx.doi.org/10.12989/scs.2017.25.6.693.

Allen, H.G. and Bulson, P.S., (1980), *Background to Buckling*, McGraw Hill, London, England.

Bapat, A.V. and Venkatramani, N. (2010), "A new approach for the representation of a point support in the analysis of plates", *J. Sound Vib.*, **120**, 107-125. https://doi.org/10.1016/0022-460X(88)90337-9.

Bathe, K.J. and Suvranu, D.E. (2001), "The method of finite spheres with improved numerical integration", *Comput. Struct.*, **79**, 2183-2196. https://doi.org/10.1016/S0045-7949(01)00124-9.

Bellifa, H., Bakora, A., Tounsi, A., Bousahla, A. A. and Mahmoud, S. R. (2017), "An efficient and simple four variable refined plate theory for buckling analysis of functionally graded plates", *Steel Compos. Struct.*, **25**(3), 257-270. http://dx.doi.org/10.12989/scs.2017.25.3.257.

Belytschko, T., Lu, Y.Y. and Gu, L. (1994), "Element free Galerkin method", *J. Numeric. Methods Eng.*, **37**, 229-256. https://doi.org/10.1002/nme.1620370205.

Bourada, F., Amara, K., Bousahla, A. A., Tounsi, A. and Mahmoud, S. R. (2018), "A novel refined plate theory for stability analysis of hybrid and symmetric S-FGM plates", *Struct. Eng. Mech.*, **68**(6), 661-675. http://dx.doi.org/10.12989/sem.2018.68.6.661.

Chen, J., Tang, W., Huang, P. and Xu, L. (2016), "A mesh-free analysis method of structural elements of engineering structures based on B-spline wavelet basis function", *Struct. Eng. Mech.*, **57**(2).

Chikh, A., Tounsi, A., Hebali, H. and Mahmoud, S. R. (2017), "Thermal buckling analysis of cross-ply laminated plates using a simplified HSDT", *Smart Struct. Syst.*, **19**(3), 289-297. http://dx.doi.org/10.12989/sss.2017.19.3.289.

Dastjerdi, R.M. (2016), "Wave propagation in functionally graded composite cylinders reinforced by aggregated carbon nanotube", *Struct. Eng. Mech.*, **57**(3), 441-456.

Do, V.N.V. and Lee, C.H. (2018), "Quasi-3D higher-order shear deformation theory for thermal buckling analysis of FGM plates based on a meshless method", *Aerosp. Sci. Tech.*, **82**, 450-465. https://doi.org/10.1016/j.ast.2018.09.017.

Duarte, C.A.M. and Oden, J.T. (1995), "Hp clouds-a meshless method to solve boundary-value problems", Technical Report 95-05; TICAM, The University of Texas, Austin, USA, May.

Garcia, O., Fancello, E.A., Barcellos, S.D. and Duarte, C.A. (2000), "Hp-Clouds in Mindlin's thick plate model", *J. Numeric. Methods Eng.*, **47**, 1381-1400.

Hedayati, P., Azhari, M., Shahidi, A.R. and Bradford, M.A., (2007), "On the use of the Lagrange multiplier technique for the unilateral local buckling of point-restrained plates, with application to side-plated concrete beams in structural retrofit", *J. Struct. Eng. Mech.*, **26**, 673-685.

Irons, B.M. (1969), "A conforming quartic triangular element for plate bending", *J. Numeric. Method. Eng.*, **1**, 29-45. https://doi.org/10.1002/nme.1620010104.

Jamshidi, S., Azhari, M. and Amoushahi, H. (2015), "Free vibration of plates of various shapes with intermediate point supports by the Hp-Cloud Method and Lagrange Multiplier", *J. Struct. Stability Dynam.*, **16**, https://doi.org/10.1142/S0219455415500558.

Kadari, B., Bessaim, A., Tounsi, A., Heireche, H., Bousahla, A.A. and Houari, M.S.A. (2018), "Buckling analysis of orthotropic nanoscale plates resting on elastic foundations", *J. Nano Res.*, **55**, 42-56. https://doi.org/10.4028/www.scientific.net/JNanoR.55.42.

Krysl, P. and Belytschko, T. (1995), "Analysis of thin plates by the element-free Galerkin method", *Comput. Mech.*, **17**, 26–35. https://doi.org/10.1007/BF00356476.

Lancaster, P. and Salkauskas, K. (1981), "Surfaces generated by moving least squares methods", *Math. Comput. Model.*, **37**, 141-158. https://doi.org/10.1090/S0025-5718-1981-0616367-1.

Lei, Z. and Zhang, Y. (2018), "Characterizing buckling behavior of matrix-cracked hybrid plates containing CNTR-FG layers", *Struct. Eng. Mech.*, **28**(4), 495-508. http://dx.doi.org/10.12989/scs.2018.28.4.495.

Li, R., Tian, Y., Wang, P, Shi, Y. and Wang, B. (2016), "New analytic free vibration solutions of rectangular thin plates resting on multiple point supports", *J. Mech. Sci.*, **110**, 53-61. https://doi.org/10.1016/j.ijmecsci.2016.03.002.

Liu, G.R. and Gu, Y.T. (2005), *An Introduction to Mesh-free*

Methods and Their Programming, Springer, New York, NY, USA.

Liu, G.R. and Liu, M.B. (2003), *Smoothed Particle Hydrodynamics a Meshfree Particle Method*, World Scientific Pub. Co. Inc., 5 Toh Tuck Link, Singapore.

Melenk, J.M. and Babuska, I. (1996), "The partition of unity finite element method, basic theory and applications", *Comput. Methods Appl. Mech. Eng.*, **139**, 289-314. https://doi.org/10.1016/S0045-7825(96)01087-0.

Menasria, A., Bouhadra, A., Tounsi, A., Bousahla, A. A. and Mahmoud, S. R. (2017), "A new and simple HSDT for thermal stability analysis of FG sandwich plates", *Steel Compos. Struct.*, **25**(2), 157-175. http://dx.doi.org/10.12989/scs.2017.25.2.157.

Meziane, M. A. A., Abdelaziz, H. H. and Tounsi, A. (2014), "An efficient and simple refined theory for buckling and free vibration of exponentially graded sandwich plates under various boundary conditions", *J. Sandwich Struct. Mater.*, **16**(3), 293-318. https://doi.org/10.1177/1099636214526852.

Naghsh, A., Azhari, M. and Saadatpour, M.M. (2018), "Thermal buckling analysis of point-supported laminated composite plates in unilateral contact", *Appl. Math. Model.*, **56**, 564-583. https://doi.org/10.1016/j.apm.2017.12.020.

Nowacki, W. (1953), "Vibration and buckling of rectangular plates simply supported at the periphery and several points inside", *Archiwum Mechaniki Stosowanej*, **5**, 437-454.

Saadatpour, M.M., Azhari, M. amd Bradford, M.A. (1998), "Buckling of arbitrary quadrilateral plates with intermediate supports using the Galerkin method", *Comput. Methods Appl. Mech. Eng.*, **164**, 297-306. https://doi.org/10.1016/S0045-7825(98)00030-9.

Shepard, D.A. (1968), "Two-dimensional interpolation function for irregularly spaced data", *Proc 23rd Nat Conf ACM*, New York, NY, USA. https://doi.org/10.1145/800186.810616.

solution to buckling and vibration problems of orthotropic plates", *Eng. Analysis Boundary Element.*, **37**(3), 579-584. https://doi.org/10.1016/j.enganabound.2013.01.007.

Suvranu, D.E. and Bathe, K.J. (2001), "Towards an efficient meshless computational technique: the method of finite spheres", *Eng. Comput.*, **18**, 170-192. https://doi.org/10.1108/02644400110365860

Suvranu, D.E. and Bathe, K.J., (2000), "The method of finite spheres", *Comput. Mech.*, **25**, 329-345. https://doi.org/10.1007/s004660050481.

Szilard, R. (2004), *Theories and Applications of Plate Analysis*, John Wiley and Sons. Inc., Hoboken, New Jersey, USA.

Tan, H.K.V., Bettess, P. and Bettess, J.A. (1983), "Elastic buckling of isotropic triangular flat plates by finite elements", *Appl. Math. Model.*, **7**, 311-316. https://doi.org/10.1016/0307-904X(83)90130-0.

Taylor, J.L. (1967), "Buckling and vibration of triangular flat plates", *J. Royal Aeronautic. Soc.*, **71**, 682-727. https://doi.org/10.1017/S0001924000054415.

Topal, U., Nazarimofrad, E. and Kholerdi, S.E.S. (2018), "Shear buckling analysis of cross-ply laminated plates resting on Pasternak foundation", *J. Numeric. Methods Eng.*, **68**(3), 369-375.

Tripathy, B. and Suryanarayan, S. (2008), "Vibration and buckling characteristics of weld-bonded rectangular plates using the flexibility function approach", *J. Mech. Sci.*, **50**, 1486-1498. https://doi.org/10.1016/j.ijmecsci.2008.08.005.

Tsiatas, G.C. and Yiotis, A.J. (2013), "A BEM-based meshless

Venugopal, N., Shastry, B.P. and Rao, G.V. (1989), "Stability of square plates resting on four symmetrically placed point supports on diagonals", *Comput. Struct.*, **31**, 293-295. https://doi.org/10.1016/0045-7949(89)90233-2.

Wang, C.M. and Liew, K.M. (1994), "Buckling of triangular plates under uniform compression", *Eng. Struct.*, **16**, 43-50. https://doi.org/10.1016/0141-0296(94)90103-1.

Wittrick, W.H., (1954), "Symmetrical buckling of right-angled isosceles triangular plates", *Aeronautical Quarterly*, **5**(2), 131-143. https://doi.org/10.1017/S0001925900001141.

Yosida, K. (1978), *Fuctional Anal.*, Springer-Verlag, Heidelberg, Berlin, Germany.

Zhang, L.W., Zhu, P. and Liew, K.M. (2014), "Thermal buckling of functionally graded plates using a local Kriging meshless method", *Compos. Struct.*, **108**, 472-492. https://doi.org/10.1016/j.compstruct.2013.09.043.

PL